



THIS MANUSCRIPT HAS BEEN SUBMITTED TO THE JOURNAL OF GLACIOLOGY AND HAS NOT BEEN PEER-REVIEWED.

What can radar-based measures of subglacial hydrology tell us about basal shear stress? A case study at Thwaites Glacier, West Antarctica

Journal:	<i>Journal of Glaciology</i>
Manuscript ID	JOG-23-0099.R2
Manuscript Type:	Article
Date Submitted by the Author:	17-Dec-2023
Complete List of Authors:	Haris, Rohaiz; Georgia Institute of Technology, School of Earth and Atmospheric Sciences Chu, Winnie; Georgia Institute of Technology, School of Earth and Atmospheric Sciences Robel, Alexander; Georgia Institute of Technology, School of Earth and Atmospheric Sciences
Keywords:	Radio-echo sounding, Subglacial processes, Ice-sheet modelling
Abstract:	Ice sheet models use observations to infer basal shear stress, but the variety of methods and datasets available has resulted in a wide range of estimates. Radar-based metrics such as reflectivity and specularity content have been used to characterize subglacial hydrologic conditions that are linked to spatial variations in basal shear stress. We explore whether radar metrics can be used to inform models about basal shear stress. At Thwaites Glacier, West Antarctica, we sample basal shear stress inversions across a wide range of ice sheet models to see how the basal shear stress distribution changes in regions of varying relative reflectivity and specularity content. Our results reveal three key findings: (1) Regions of high specularity content exhibit lower mean basal shear stresses (2) Wet and bumpy regions, as characterized by high relative reflectivity and low specularity content, exhibit higher mean basal shear stresses (3) Models disagree about what basal shear stress should be at the onset of rapid ice flow and high basal melt where relative reflectivity

	and specularity content are low.

SCHOLARONE™
Manuscripts

1 What can radar-based measures of subglacial hydrology tell 2 us about basal shear stress? A case study at Thwaites 3 Glacier, West Antarctica

4 Rohaiz HARIS,¹ Winnie CHU,¹ Alexander ROBEL¹

5 ¹*School of Earth and Atmospheric Sciences, Georgia Institute of Technology*

6 *Correspondence: Rohaiz Haris <rharis3@gatech.edu>*

7 **ABSTRACT.** Ice sheet models use observations to infer basal shear stress,
8 but the variety of methods and datasets available has resulted in a wide range
9 of estimates. Radar-based metrics such as reflectivity and specularity content
10 have been used to characterize subglacial hydrologic conditions that are linked
11 to spatial variations in basal shear stress. We explore whether radar metrics
12 can be used to inform models about basal shear stress. At Thwaites Glacier,
13 West Antarctica, we sample basal shear stress inversions across a wide range
14 of ice sheet models to see how the basal shear stress distribution changes
15 in regions of varying relative reflectivity and specularity content. Our results
16 reveal three key findings: (1) Regions of high specularity content exhibit lower
17 mean basal shear stresses (2) Wet and bumpy regions, as characterized by high
18 relative reflectivity and low specularity content, exhibit higher mean basal
19 shear stresses (3) Models disagree about what basal shear stress should be at
20 the onset of rapid ice flow and high basal melt where relative reflectivity and
21 specularity content are low.

22 1 INTRODUCTION

23 Glaciers and ice streams discharge ice from the interior of the Antarctic Ice Sheet to the ocean at a rate
24 which is largely controlled by conditions at the ice-bed interface (Schoof, 2007). The influence of subglacial

Haris and others:

25 conditions on basal friction - and by extension on ice flow - is key to modeling the future potential evolution
26 of the Antarctic ice sheet. Direct borehole observations over small areas of the ice sheet have been used to
27 characterize the ice-bed interface by studying subglacial hydrologic systems (Hubbard and others, 1995) and
28 basal friction (Pfeffer and others, 2000), but repeating these direct observations over the entire Antarctic
29 Ice Sheet is logistically challenging. As such, alternative geophysical observational methods and forward
30 models are typically used to analyze basal conditions over spatially extensive regions. Geophysical methods,
31 such as seismic reflection (King, 2004) and radar sounding (Dowdeswell and Evans, 2004), are useful tools to
32 indirectly characterize the ice-bed interface by inferring the locations of subglacial water (Chu and others,
33 2016), distribution of basal channels (Schroeder and others, 2013), and bed morphology (Smith, 1997).
34 However, most individual geophysical surveys are limited to the local glacier scale and there are only a
35 handful of repeated surveys (e.g., NASA Operation IceBridge) that cover larger areas of the Antarctic Ice
36 Sheet.

37 Due to the lack of extensive physical observations on a catchment scale, basal shear stress is typically
38 inferred from remote sensing observations (typically surface velocity and ice thickness) using control or data-
39 assimilation methods (MacAyeal, 1993). However, the inferred basal shear stress is sensitively dependent
40 on the details of the input dataset, the choice of the sliding law, the control method, and regularizations
41 therein (Morlighem and others, 2010; Seroussi and others, 2013; Sergienko and Hindmarsh, 2013; Zhao and
42 others, 2018). As a result, for the same area of an ice sheet, inversions can give a wide range of estimates
43 for basal shear stress (Seroussi and others, 2020).

44 Inversions can be unstable, as a small amount of error or change in observations can lead to large
45 differences in modeled parameters. Input observational datasets inherently have a small amount of error
46 that can result in inversions trying to overfit the observations below the level of error in measurements.
47 Furthermore, the transfer function relating variability in basal conditions to surface velocity or slope
48 is a low-pass filter, resulting in surface properties responding to basal properties averaged over several
49 ice thicknesses (Gudmundsson, 2003; Wolovick and others, 2023). As such, widely differing basal drag
50 fields can reproduce similar surface velocities (Habermann and others, 2012) which makes inversions ill-
51 posed when inferring basal shear stress from observations of surface velocities (Wolovick and others, 2023).
52 Regularizations help to stabilize the inversion solution by imposing additional constraints that bias the
53 solution and reduce overfitting. A common regularization method is the Tikhonov regularization, which
54 determines how much weight to give to the cost function and can give preference to a solution with

55 desirable properties (Habermann and others, 2012). To make an informed decision in choosing and adjusting
56 regularization terms, it is therefore important to constrain bed characteristics, roughness, and subglacial
57 hydrology.

58 Previous studies have characterized subglacial hydrology using other observable geophysical methods
59 and investigated their relationship with basal friction. Kyrke-Smith and others (2017) utilized seismic
60 profiles to infer acoustic impedance in order to estimate mechanical basal conditions. Comparisons between
61 the seismic observations and high resolution basal shear stress inversions show that there is a stronger
62 correlation between acoustic impedance and basal slipperiness or basal drag at scales longer than the ice
63 thickness (>7 km) compared to smaller scales. Other studies have used airborne radar sounding to infer
64 characteristics and spatial variations of subglacial hydrology using bed reflectivity (i.e., brightness of bed
65 echo returns) and specularity content (i.e., relative contribution of specular (mirror-like reflections) signals
66 to the total returned bed energy) (Schroeder and others, 2013; Chu and others, 2021). Das and others
67 (2023) conducted correlation experiments and found no strong correlation between relative reflectivity and
68 the sliding-law parameter used to control basal friction in numerical ice sheet models. These studies have
69 suggested a potential link between the spatial distribution of subglacial hydrology and basal shear stress
70 based on geophysical observations. In this study, we examine the statistical relationship between radar
71 metrics and basal shear stress in more detail by combining numerical ice sheet models and a high resolution
72 radar sounding dataset from the Amundsen Sea Sector in West Antarctica. Our study site is Thwaites
73 Glacier, located in the Amundsen Sea Embayment, which is a dominant contributor to Antarctic Ice Sheet
74 mass loss (Pritchard and others, 2009).

75 **2 DATA AND METHODS**

76 **2.1 Radar Sounding Observations**

77 We use published radar bed reflectivity and specularity content observations from two airborne radar
78 sounding studies to characterize subglacial hydrologic conditions at Thwaites Glacier (Chu and others,
79 2021; Schroeder and others, 2013). The radar metrics were calculated from radar sounding data measured
80 by the High Capability Airborne Radar Sounder (HiCARS) system with a 60 MHz center frequency and 15
81 MHz bandwidth (Peters and others, 2007). The data was collected as part of a campaign that conducted
82 airborne radar sounding surveys of the Amundsen Sea Embayment during the 2004/2005 austral field
83 season (Holt and others, 2006; Vaughan and others, 2006).

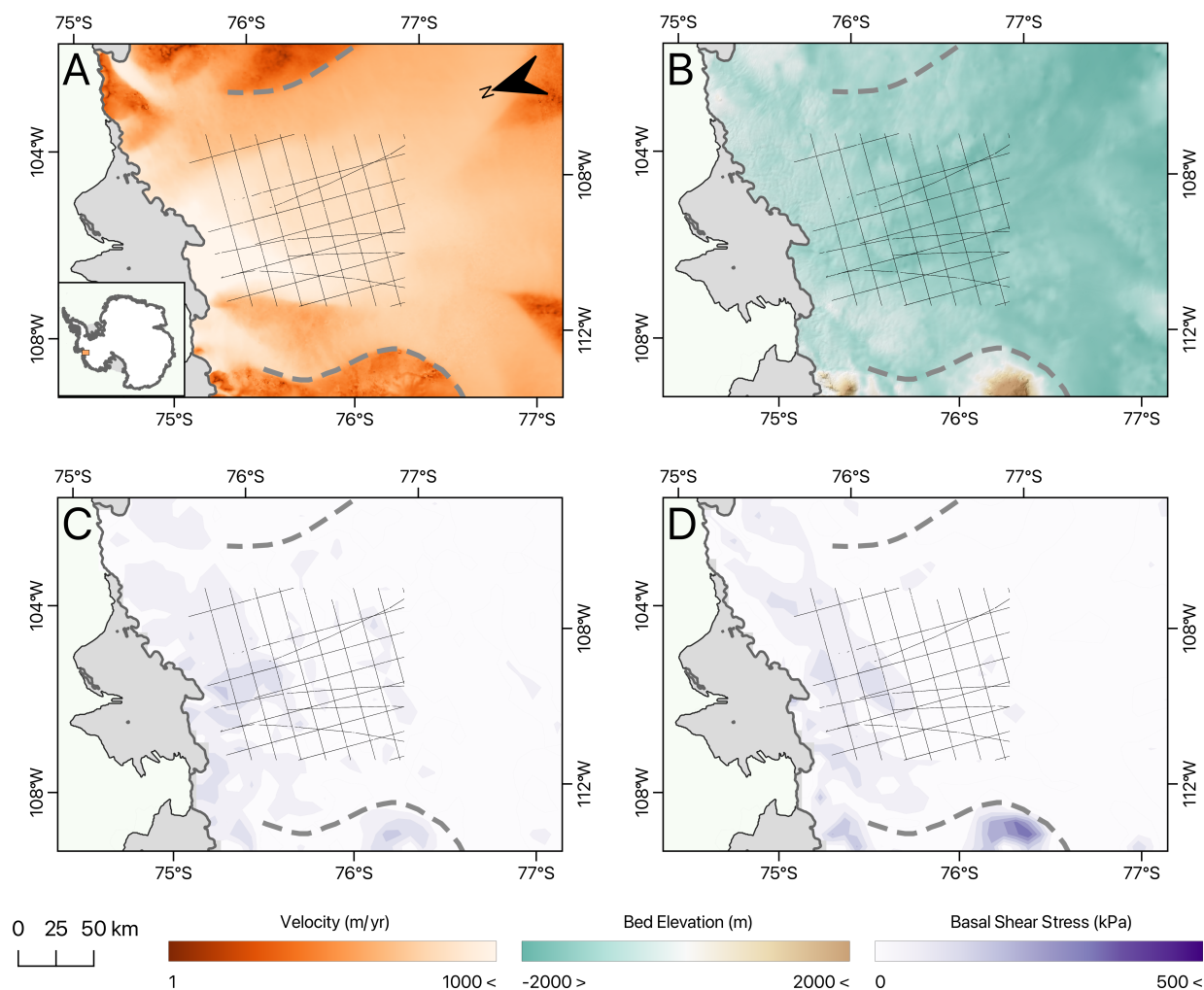


Fig. 1. Site Map indicating radar flight tracks (black line) (Chu and others, 2021), shear margin (dotted grey line) (Schroeder and others, 2013), with (A) MEaSUREs ice velocity (Rignot and University Of California Irvine, 2017; Mouginot and others, 2017) using a logarithmic colorscale, (B) BedMachine v3 bed topography (Morlighem and others, 2020; Morlighem, 2022) & REMA hillshade (Howat and others, 2022), (C) NCAR CISM basal shear stress inversion (Lipscomb and others, 2019; Seroussi and others, 2020) and (D) JPL1 ISSM basal shear stress inversion (Seroussi and others, 2020)

84 Bed reflectivity describes the brightness of returned bed echoes and is mostly influenced by the difference
85 in dielectric permittivity between two materials (Peters, 2005). A vertical transition between ice and liquid
86 freshwater results in a 10 - 15 dB increase in reflectivity relative to the surrounding ice-bed interface
87 (Peters, 2005; Chu and others, 2016; Young and others, 2016). Other material properties such as electrical
88 conductivity can also impact reflectivity (Tulaczyk and Foley, 2020). We use relative reflectivity (relative
89 to our study site as seen in Figure 3B) from Chu and others (2021) which captures spatial variations within
90 a study site as opposed to absolute reflectivity which is influenced by many unknown parameters specific
91 to the site (Peters and others, 2007; Chu and others, 2021). We refer readers to Chu and others (2021) for
92 more details of the reflectivity dataset used in our study.

93 Specularity content is a measure of the angular distribution of the bed echo power, with values ranging
94 from 0 to 1 and is computed by finding the fraction of the total returned radar energy that is returned in
95 a narrow angular distribution around the specular direction compared to energy diffusely scattered. We
96 refer readers to Schroeder and others (2013) for more details of the specularity content dataset used in
97 our study. Differences in ice-bedrock interface geometry produce unique scattering signatures that can be
98 used to characterize interface roughness and subglacial hydrology. Thus, specularity content is typically
99 interpreted to indicate a change in interface roughness (Schroeder and others, 2013). Smooth interfaces
100 will return sharp mirror-like reflections. This results in higher specularity content values (>0.3) that are
101 thought to be indicative of a smooth interface such as a region of low bed roughness or subglacial lakes with
102 flat surfaces. Conversely, diffuse interfaces will scatter energy in all directions and have a low specularity
103 content (<0.3) (Schroeder and others, 2013; Young and others, 2016; Chu and others, 2021).

104 The goal of our study is not to definitively distinguish between the influence of bed roughness versus
105 material contrast on bed reflectivity or specularity content; but to explore whether these radar metrics
106 correspond to any changes in basal shear stress suggested by ice sheet models. This is also the reason
107 why we choose to combine both relative reflectivity and specularity content (each sensitive to a different
108 degree to the presence of subglacial water or changes in bed roughness) to provide a more comprehensive
109 interpretation of basal conditions at Thwaites Glacier.

110 2.2 Model-Inferred Basal Friction

111 Basal shear stress on a continental scale is typically inferred from inverse methods in ice sheet models
112 (Sergienko and others, 2008; MacAyeal, 1992; Pattyn and others, 2017) using large-scale remote sensing

Haris and others:

113 measurements such as ice velocity, surface elevation and ice thickness. We use previously published basal
114 shear stress inversions from a subset of Antarctic ice sheet model simulations included in the most recent Ice
115 Sheet Model Intercomparison project (Seroussi and others, 2020). We exclude models that have unphysical
116 values of basal shear stress or low resolution over our study site. The subset of models include: AWI PISM1
117 (Bueler and Brown, 2009; Winkelmann and others, 2011; Aschwanden and others, 2012; Seroussi and others,
118 2020), JPL1 ISSM (Seroussi and others, 2020), PIK PISM1 (Bueler and Brown, 2009; Winkelmann and
119 others, 2011; Seroussi and others, 2020), UCIJPL ISSM (Seroussi and others, 2020), UTAS ElmerIce
120 (Seroussi and others, 2020), VUB AISMPALEO (Huybrechts, 1990, 2002; Seroussi and others, 2020), DOE
121 MALI (Hoffman and others, 2018; Seroussi and others, 2020), NCAR CISM (Lipscomb and others, 2019;
122 Seroussi and others, 2020). Each modeling group participating in ISMIP6 uses their own inversion method
123 to initialize the basal sliding coefficient field, which is then held constant for the transient simulations of
124 future ice sheet behavior which are the focus of the inter-comparison exercise. Thus, this ensemble of
125 inversions is a representative sampling of the best estimates of basal shear stress which are used to predict
126 future ice sheet behavior. We have also added the inversion from Sergienko and Hindmarsh (2013) which
127 includes some finer resolution (kilometer-scale) features not present in ISMIP6 inversions.

128 Most inversions examined in this study use some variation of the control method described in MacAyeal
129 (1993) to minimize the misfit between the observed and modeled ice sheet surface velocities (Morlighem and
130 others, 2010). The control method uses a cost function and subsequent optimizations to reduce the error
131 between a forward model's output and observations such as surface velocity or topography (Ranganathan
132 and others, 2021). Different modeling groups use different variations of the cost function in MacAyeal
133 (1993) and apply their own regularizations and optimizations as well. For example, some cost functions
134 may prioritize reducing the velocity misfit in slow moving regions (Morlighem and others, 2010), while other
135 cost functions may not consider velocity direction and only reduce misfit in the magnitude of velocities
136 (Zhao and others, 2018). Other models use transient spin-up methods (Schoof, 2006; Pollard and DeConto,
137 2012) that assimilate observations to nudge the output to minimize the mismatch between modeled and
138 observed data. Ultimately, such differences in inversion methodology and input data lead to a wide range
139 of predicted basal shear stress among the models considered here. Since direct observations of basal shear
140 stress are sparse (or absent entirely in some regions, including the region we consider in this study),
141 inversions are not validated against observations. Thus, we instead consider a representative sample of
142 nine inversions and analyze where these inversions agree and disagree with each other in terms of their

143 statistical relationship to radar sounding metrics.

144 **2.3 Statistical Methods for Comparison of Radar Observations and Modeled Data**

145 Due to varying spatial resolutions of the basal shear stress inversions used in this study and the higher
146 resolution of radar data, all inversions of basal shear stress are interpolated onto the radar flight track
147 coordinates using linear interpolation. We only consider points where all inversions have estimates of basal
148 shear stress to ensure a fair comparison across inversions.

149 Prior studies (e.g., Kyrke-Smith and others (2017); Das and others (2023)) have attempted to quantify
150 the relationship between measures of subglacial hydrology and basal shear stress using regression methods
151 and generally failed to do so except at spatial scales larger than 7 km. The same is true for the radar
152 and basal shear stress data used here. We first examined the linear regression between the modeled basal
153 shear stress and the two radar indices, relative reflectivity and specularity content respectively. On a basin
154 scale, the largest Pearson correlation coefficient observed across all models was -0.3269 between JPL1 ISSM
155 basal shear stress and specularity content. While we observe a correlation between basal shear stress and
156 radar metrics using the Pearson Correlation Coefficient, conducting statistical tests on large datasets can
157 yield statistically significant results when there may be no practical relationship in reality (Johnson, 1999).
158 The significance of the correlation between basal shear stress and radar metrics can be seen to be spurious
159 as the regressions are heavily biased by the density of certain basal shear stress values in the dataset
160 (Supplementary Figures S2 & S3). In reality, basal shear stress has a very weak linear dependence on
161 radar metrics. Instead, we use sampling statistics to determine if radar metrics can be used to classify
162 regions with statistically significant variations in basal shear stress. After sub-sampling the model-based
163 values of basal shear stress using various permutations of reflectivity and specularity content thresholds
164 across the extent of the radar dataset, we analyze how the mean basal shear stress changes across different
165 inversions and different radar metric thresholds. Basal shear stress samples with less than 100 values are
166 not considered to ensure that any changes in the basal shear stress distribution are not due to individual
167 outliers within small sample sizes. We also identify where regions of significant deviation in mean basal
168 shear stress occur and how they relate to other variables such as surface ice velocity and bed topography.

169 Finally, we used two-sample Kolmogorov-Smirnov testing to verify whether sub-sampling basal shear
170 stress on the basis of radar data produces a statistically significant difference in the sub-sampled basal
171 shear stress distribution compared to randomly sampling the same number of points from the entire basal

Haris and others:

172 shear stress dataset. The two-sample Kolmogorov-Smirnov test (henceforth referred to as KS test) is a
173 hypothesis test that evaluates the difference in cumulative distribution functions (CDFs) of two datasets
174 and can be used to evaluate whether both samples share the same continuous distribution (Dimitrova and
175 others, 2020)). In KS testing, our null hypothesis is that the sub-sampled data and the overall basal shear
176 stress data share the same distribution, which would indicate that reflectivity and specularity content are
177 not useful tools for discriminating regions with different basal shear stress. Rejecting the null hypothesis for
178 a particular reflectivity and specularity content threshold is a useful way to identify regions with different
179 basal shear stresses. Samples that make up 70 percent or more of the inversion dataset are not considered
180 as these are likely to be representative of the entire dataset and have well known issues when inferring
181 the difference between distributions. The KS test is overly sensitive for large sample sizes and detects a
182 statistically significant difference between the sub-sampled data and the complete basal shear stress dataset
183 even if the actual difference is negligible (Sullivan and Feinn, 2012; Larson, 2018). Due to this sensitivity to
184 sample size, we perform the KS test on data sub-sampled on the basis of reflectivity and specularity content
185 and a random sample of the same size to avoid a Type I error which occurs when the null hypothesis is
186 rejected incorrectly.

187 **3 RESULTS**

188 We investigate whether using reflectivity and specularity content thresholds as sampling criteria produce
189 statistically significant differences in basal shear stress across a range of model inversion products. The
190 results from sub-sampling are illustrated in Figure 2 in a 50x50 grid, where each grid square reflects the
191 deviation in mean basal shear stress for a sub-sample based on either maximum or minimum thresholds of
192 specularity content and reflectivity, with respect to the mean basal shear stress over all radar flight lines.

193 Though we have calculated these basal shear stress deviations for all nine inversions considered in this
194 study, Figures 2A and 2D plot results for the NCAR CISM inversion from ISMIP6 (Seroussi and others,
195 2020) and Figures 2B and 2E plot results of the JPL1 ISSM inversion from ISMIP6 (Seroussi and others,
196 2020). In Figures 2A and 2B, we apply a combination of reflectivity and specularity content thresholds
197 to sub-sample each inversion such that for a given grid cell in the figure, we sub-sample basal shear stress
198 values that occur in regions of specularity content greater than X and relative reflectivity greater than Y
199 where X and Y correspond to the x-axis and y-axis values for that grid cell respectively. We refer to these
200 plots as "high-high" plots to indicate how the thresholds applied are "Higher than specularity content-

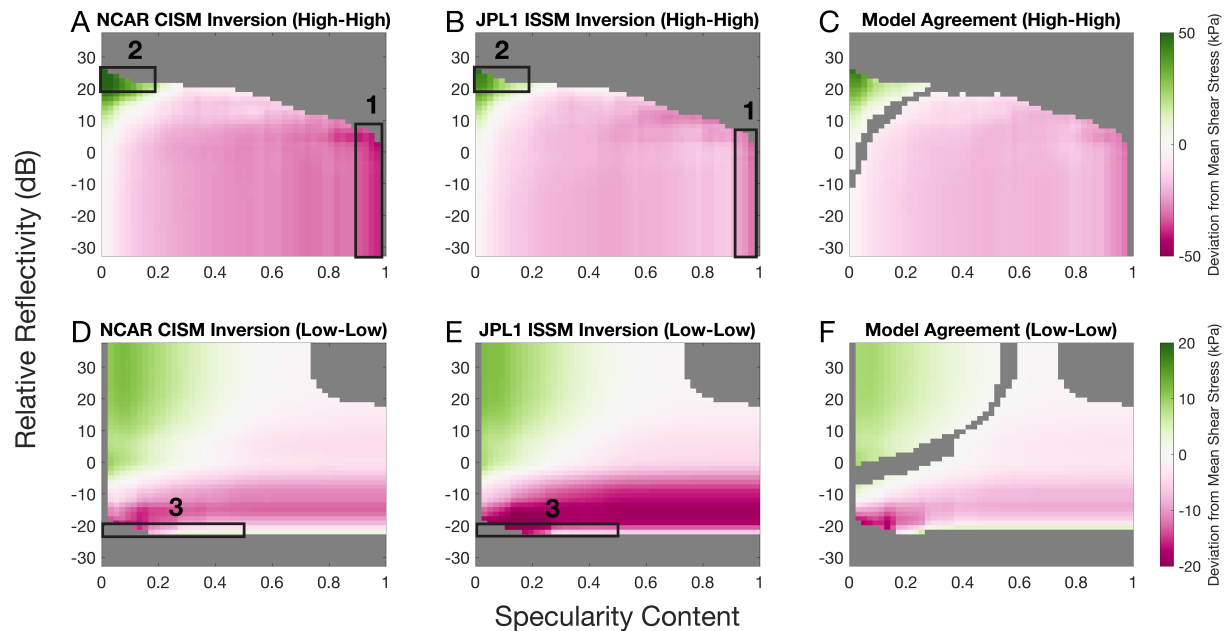


Fig. 2. 2A and 2B show the high-high plots for NCAR CISM (Lipscomb and others, 2019; Seroussi and others, 2020) and JPL1 ISSM inversion (Seroussi and others, 2020) respectively. We apply thresholds when subsampling on the basis of radar data such that for a given grid cell in the figure, we subsample basal shear stress values that occur in regions of specularity content greater than X and relative reflectivity greater than Y where X and Y correspond to the x-axis and y-axis values for that grid cell respectively. 2D and 2E show the low-low plots for the NCAR CISM inversion and JPL1 ISSM inversion respectively. We apply thresholds when subsampling on the basis of radar data such that for a given grid cell in the figure, we subsample basal shear stress values that occur in regions of specularity content lower than X and relative reflectivity lower than Y where X and Y correspond to the x-axis and y-axis values for that grid cell respectively. The colormap for 2A, 2B, 2D & 2E represent the deviation in mean basal shear stress of the sample from the overall basal shear stress distribution. Grey areas represent NaN values where there are less than 100 values or more than 70% of the dataset. Regimes of significant deviation in mean basal shear stress are identified in 2A, 2B, 2D & 2E by numbers and corresponding rectangles. Figures 2C and 2F show where seven or more inversions agreed on the sign of deviation from mean basal shear stress on the high-high plot and low-low plot respectively. The colormap indicates the inter-model mean of the deviation in mean basal shear stress for that relative reflectivity and specularity threshold. Grey areas represent NaN values where there are less than 100 values or more than 70% of the dataset, or where seven or more inversions disagreed on the sign of deviation from mean basal shear stress.

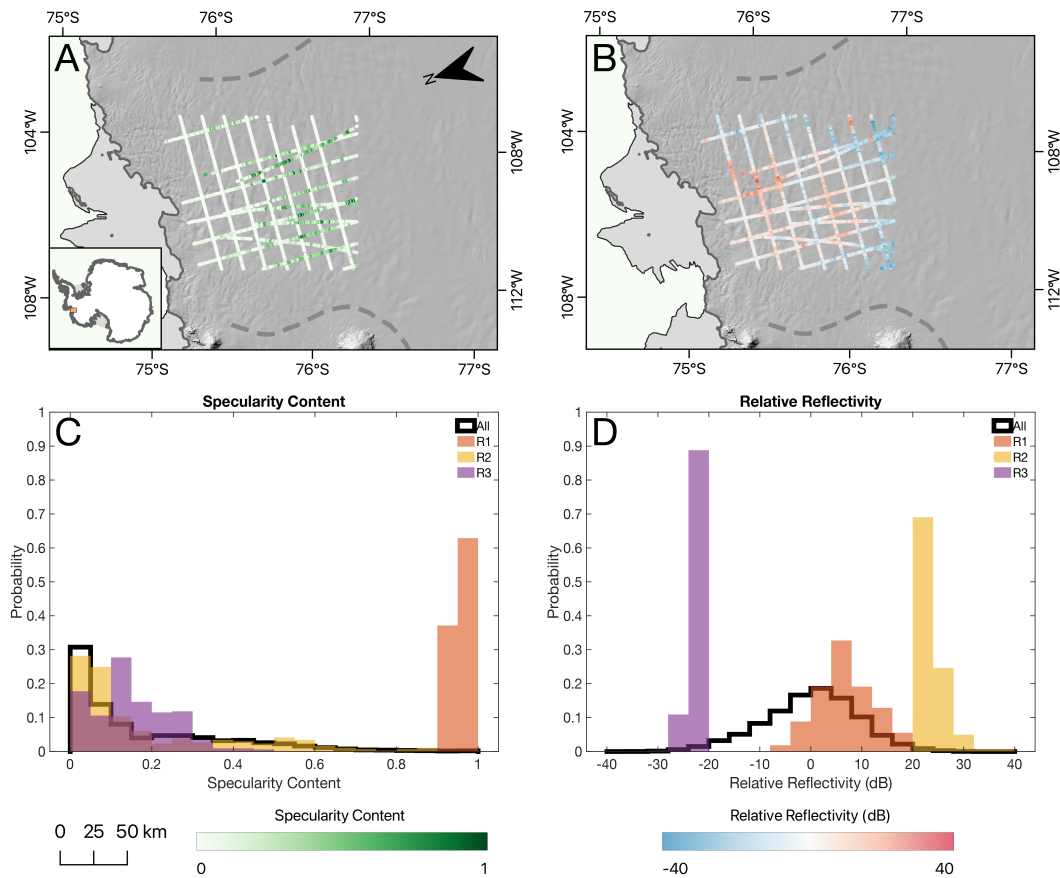


Fig. 3. 3A and 3B plot the specularity content dataset (Schroeder and others, 2013) and relative reflectivity dataset (Chu and others, 2021) respectively with REMA hillshade (Howat and others, 2022) for our study site in Thwaites Glacier, West Antarctica. 3C and 3D plot histograms of specularity content and relative reflectivity respectively. In 3C and 3D, the histogram of the overall dataset is plotted with a thick black line while the histograms of the 3 regimes are plotted with colored bars and identified in the legend.

201 higher than relative reflectivity". Conversely in Figures 2D and 2E (referred to as "low-low" plots), the
202 combination of reflectivity and specularity content thresholds applied for a given grid cell are specularity
203 content less than X and relative reflectivity less than Y where X and Y correspond to the x-axis and
204 y-axis values for that grid cell respectively. We refer to these plots as "low-low" plots to indicate how the
205 thresholds applied are "lower than specularity content-lower than relative reflectivity"

206 We identify three regimes in Figure 2 and Figure 3 where sub-sampling with reflectivity and specularity
207 content thresholds lead to a substantial and coherent deviation in mean basal shear stress across most (or
208 all nine) inversion products as verified by KS testing. While the range of spatial variation in basal shear
209 stress differs between the models, the sign of deviation in mean basal shear stress is consistent across
210 models for Regime 1 and Regime 2. Regime 1 occurs in areas where specularity content is > 0.9 , and there
211 is a significant decrease in mean basal shear stress from 1 kPa up to 67 kPa depending on the inversion
212 product. Regime 2 occurs in areas where relative reflectivity is between 20 dB and 35 dB and specularity
213 content is typically < 0.2 (though the exact reflectivity and specularity content boundaries vary depending
214 on the inversion). In this bright but diffuse bed environment, there is a significant increase in mean basal
215 shear stress from 4 kPa up to 126 kPa depending on the inversion product. Finally, regime 3 occurs in dim
216 bed areas where relative reflectivity is < -20 dB and specularity content < 0.5 where there is a significant
217 deviation in mean basal shear stress across all inversions. However, inversions disagree on the sign of
218 this deviation in mean basal shear stress. Three inversions indicate a significant increase in mean basal
219 shear stress from 3 kPa up to 155 kPa depending to the inversion product. Conversely, the remaining six
220 inversions indicate a significant decrease in mean basal shear stress from 2 kPa up to 21 kPa depending on
221 the inversion product.

222 4 DISCUSSION

223 In regions of high specularity content (Regime 1 identified in Figure 2A, 2B, 3C, 3D), a lower mean basal
224 shear stress was observed across all inversions. Reflected radar energy from smooth ice-bedrock interfaces
225 is specular due to minimal scattering (Schroeder and others, 2015; Young and others, 2016). Regions of
226 high specularity content have also been proposed as the location of broad canals incised into the subglacial
227 till below Thwaites Glacier (Schroeder and others, 2013) or spatially continuous subglacial water sheets,
228 which are both thought to reduce basal friction over large regions (Walder and Fowler, 1994; Creyts and
229 Schoof, 2009).

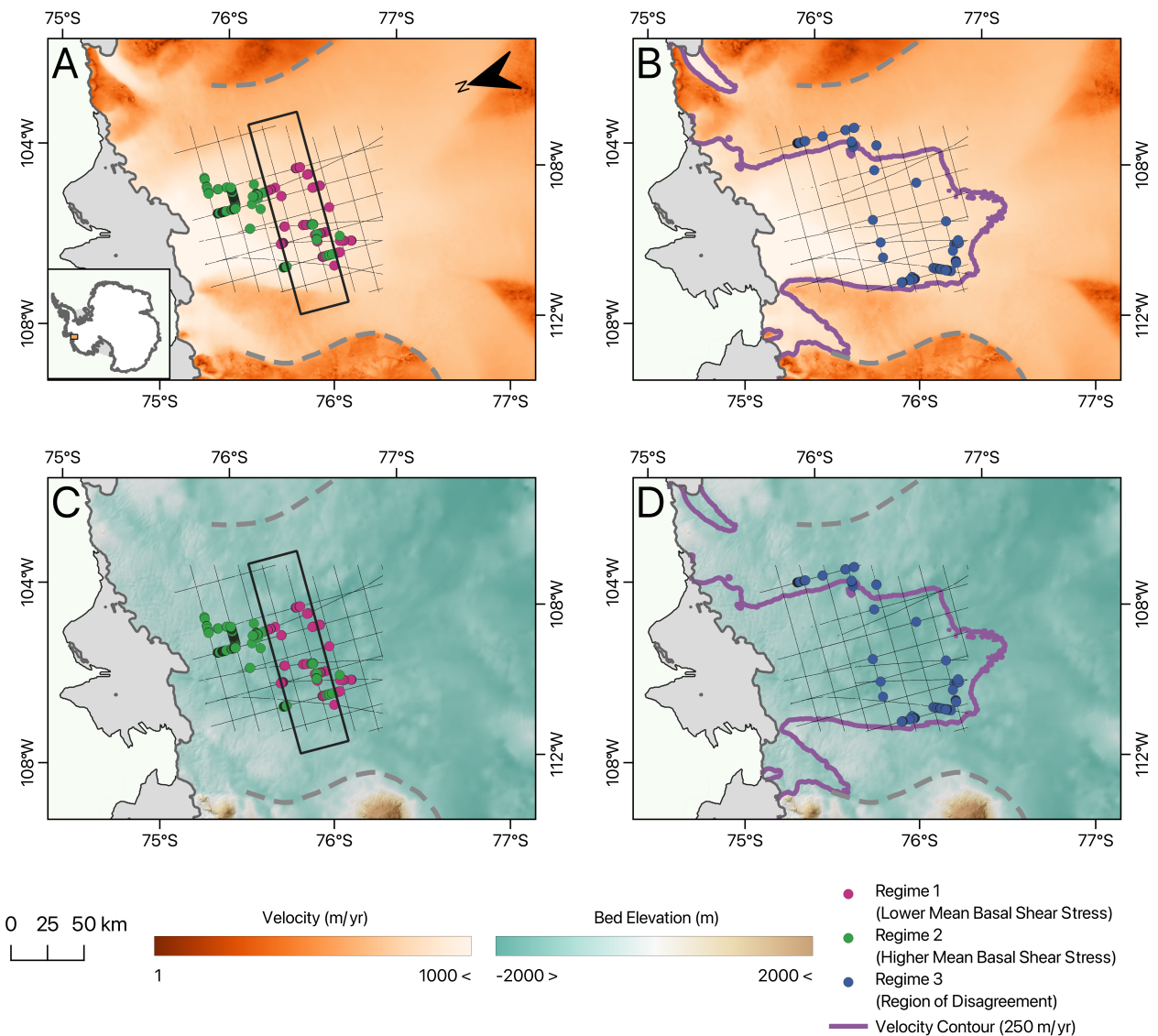


Fig. 4. Spatial plot to observe variations in regions of significant deviation in mean basal shear stress. (A) Regime 1 where there is high specularity content (pink scatter markers showing lower mean basal shear stress) and Regime 2 where there is high reflectivity and low specularity content (green scatter markers showing higher mean basal shear stress) with MEaSUREs ice velocity plotted with a logarithmic colorscale (Rignot and University Of California Irvine, 2017; Mouginot and others, 2017), (B) Regime 3 where there is low reflectivity and low specularity (blue scatter markers indicating disagreement between models on what basal shear stress should be) with MEaSUREs ice velocity plotted with a logarithmic colorscale. (C) Region 1 and Region 2 with BedMachine v3 bed topography (Morlighem and others, 2020; Morlighem, 2022) and REMA hillshade (Howat and others, 2022), (D) Regime 3 with BedMachine v3 bed topography and REMA hillshade. The box in (A) and (C) represents our identified transition from a distributed to channelized system accompanied by an increase in mean basal shear stress. The purple contour line in (B) and (D) represents where ice velocity is 250 m yr⁻¹.

230 Regions of low specularity content and high reflectivity (Regime 2 identified in Figure 2A, 2B, 3C, 3D)
231 show a higher mean basal shear stress across all inversions. The combination of low specularity content and
232 high reflectivity is thought to be indicative of wet regions with a rough ice surface, which would be seen
233 in concentrated R othlisberger channels of water incised upward into the basal glacier ice (Schroeder and
234 others, 2013). Such concentrated channels reduce the water flow through extensive distributed drainage
235 systems, and so are thought to increase basal friction on average (Schoof, 2010), which is consistent with
236 our findings of higher mean basal shear stress in these regions.

237 Regions of high specularity content and lower mean basal shear stress are located in the upstream
238 reaches of the Thwaites catchment, while regions of low specularity content, high reflectivity and higher
239 mean basal shear stress are mostly located in the downstream reaches of the Thwaites catchment. It has
240 been theorized that the transition from a distributed to channelized water system at Thwaites Glacier is
241 accompanied by an increase in basal shear stress (Schroeder and others, 2013). Our results are consistent
242 with this prior hypothesis where we see an increase in mean basal shear stress from Regime 1 to Regime
243 2. We independently identify this transition in Figure 4A and 4C which is consistent with the transition
244 identified in Schroeder and others (2013).

245 Regions of low reflectivity and low specularity content (Regime 3 identified in Figure 2D, 2E, 3C, 3D)
246 are indicative of a dry bed and show strong deviations from mean basal shear stress over the whole Thwaites
247 study within particular inversions, but the sign of the deviation is not consistent between inversions. Three
248 inversions considered in this study have high basal shear stress in low reflectivity and low specularity
249 content regions, while the other six inversions have low basal shear stress. This region of disagreement
250 between inversions is occurring at the onset of rapid ice flow and high basal melt (i.e., where ice velocity
251 is approximately 250 m yr^{-1} in Fig 4B and 4D denoted by the purple contour). The location of onset
252 of rapid flow is known to vary widely between models due to generally inadequate treatments of the
253 thermo-mechanical conditions in ice stream onset regions (Mantelli and others, 2019; Mantelli and Schoof,
254 2019). Models taking part in ISMIP6 may also differ on the location of streaming ice flow due to differing
255 horizontal resolution or ice flow approximations (Payne and others, 2000; Hindmarsh, 2009). We thus
256 identify a distinct radar signature of low reflectivity and low specularity content (Regime 3 in Figures 3C
257 and 3D) for the location of onset rapid ice flow where models disagree on the sign of deviation in mean
258 basal shear stress.

259 We also identify two additional regimes of deviation in mean basal shear stress that is observed across

Haris and others:

260 all models; a regime of low specularity (green arm of the "L" found in Figures 2D & 2E) and a regime of
261 low reflectivity (red arm of the "L" found in Figures 2D & 2E). A large fraction of the overall dataset is
262 located in these two regimes. As a result, we do not focus our analysis on these regimes as they do not
263 provide a useful criteria for sub-sampling basal shear stress inversions.

264 Other studies have also investigated the correspondence between indirect geophysical measures of sub-
265 glacial hydrology to basal shear stress. Das and others (2023) calculated correlations between radar re-
266 flectivity and sliding law parameter (representative of basal friction) for three models and were unable
267 to find a strong correlation. Kyrke-Smith and others (2017) found that there may not be a discernible
268 relationship between subglacial hydrology and basal shear stress at short length scales (below 7 km), as
269 they observed no correlation between acoustic impedance and basal shear stress within seismic profiles.
270 However, a stronger correlation was observed when values were averaged over an ice thickness scale and
271 distinct profiles were compared. Our study is consistent with the conclusions of Das and others (2023)
272 and Kyrke-Smith and others (2017). We were unable to find a statistically significant relationship between
273 basal shear stress and reflectivity or specularity content using regression techniques across radar profiles.

274 However, we do identify at least two useful radar metric thresholds for identifying regions of substantial
275 deviations in basal shear stress which are statistically distinct from random sampling of basal shear stress
276 data. This novel approach has also revealed that regions of low relative reflectivity and low specularity
277 content indicative of a dry bed consistently occur at the zone of Thwaites Glacier where ice starts to flow
278 fast. However, basal shear stress inversions tend to disagree about the basal shear stress in this region, thus
279 requiring better constraints to be able to model ice flow in this region more accurately. The relationship
280 between subglacial hydrology and basal shear stress may not be apparent at short length scales which
281 are filtered out by ice sheet dynamics (Raymond and Gudmundsson, 2005) and may not be apparent in
282 surface velocity which is the main constraint for basal shear stress inversions. Many sliding laws quantify
283 the relationships between ice velocity, basal shear stress and basal water pressure. However, other factors
284 may also play a role in controlling basal sliding, and radar sounding provides independent constraints on
285 those factors that may not be captured by current inversion methods.

286 **5 CONCLUSION**

287 Different ice sheet models use different methods and datasets to estimate basal shear stress. In this study,
288 we have shown that there are broad relationships between basal shear stress as determined by velocity

289 inversions and radar metrics across models and locations within our study site at Thwaites Glacier, West
290 Antarctica. We also use radar sounding to identify regions of low relative reflectivity and low specular-
291 ity content characterized by a unique radar signature where models produce widely differing constraints on
292 basal shear stress.

293 Presently, ice velocity and thickness are the main constraints for inversions. The results of this study
294 indicate that radar sounding can potentially provide an independent constraint on subglacial properties
295 that have been previously theorized to influence basal shear stress. However, ground-truth constraints
296 from borehole measurements of basal shear stress or other methods are necessary since the relationships
297 identified in this study are themselves based on existing inversions. We also find that reflectivity and spec-
298 ularity content contain spatial variations that cannot be explained by current basal shear stress estimates
299 derived from ice velocity alone, thus indicating that they may contain additional information that could
300 be valuable to models, e.g., using subglacial hydrology models. Constraints based on thresholds in radar
301 metric data could be incorporated into control methods using inequality constraints, for which there are
302 existing optimization methods (Bryson and others, 1963). While results from this study have shown that
303 radar can be useful in providing constraints on factors not yet captured by inversions, further work on data
304 assimilation into ice sheet models is required before radar sounding metrics can be used directly to inform
305 ice-flow models on subglacial conditions.

306 **6 DATA AVAILABILITY**

307 The code used in this study can be found on Github (https://github.com/rohaizharis/inversion_radar2022).
308 The bed reflectivity data is from Chu and others (2021) and specular-ity content data is from Schroeder
309 and others (2013). The processed radargrams and derived parameters from Chu and others (2021) can be
310 found on the USAP-DC (<https://doi.org/10.15784/601436>). The inversions used in this study are from
311 Sergienko and Hindmarsh (2013) and Seroussi and others (2020). The interpolated data for use with the
312 code can be found on Zenodo (<https://doi.org/10.5281/zenodo.10391022>). The surface ice velocity from
313 MEaSURES (Rignot and University Of California Irvine, 2017; Mouginot and others, 2017), bed topogra-
314 phy from BedMachine v3 (Morlighem and others, 2020; Morlighem, 2022), surface elevation hillshade from
315 REMA (Howat and others, 2022), can be found online.

316 **7 ACKNOWLEDGMENTS**

317 All authors were supported using startup funds from Georgia Institute of Technology. We would like to
318 thank Vincent Verjans, Ziad Rashed, Angelo Tarzona and Kiera Tran for their feedback on the figures
319 shown. We would also like to thank editor Dustin Schroeder and two anonymous reviewers for their
320 constructive feedback that helped to improve the manuscript.

321 **REFERENCES**

- 322 Aschwanden A, Bueler E, Khroulev C and Blatter H (2012) An enthalpy formulation for glaciers and ice sheets.
323 *Journal of Glaciology*, **58**(209), 441–457, ISSN 0022-1430, 1727-5652 (doi: 10.3189/2012JoG11J088)
- 324 Bryson AE, Denham WF and Dreyfus SE (1963) Optimal programming problems with inequality constraints. *AIAA*
325 *Journal*, **1**(11), 2544–2550, ISSN 0001-1452, 1533-385X (doi: 10.2514/3.2107)
- 326 Bueler E and Brown J (2009) Shallow shelf approximation as a “sliding law” in a thermomechanically coupled
327 ice sheet model. *Journal of Geophysical Research: Earth Surface*, **114**(F3), 2008JF001179, ISSN 0148-0227 (doi:
328 10.1029/2008JF001179)
- 329 Chu W, Schroeder DM, Seroussi H, Creyts TT, Palmer SJ and Bell RE (2016) Extensive winter subglacial water
330 storage beneath the Greenland Ice Sheet. *Geophysical Research Letters*, **43**(24), ISSN 0094-8276, 1944-8007 (doi:
331 10.1002/2016GL071538)
- 332 Chu W, Hilger AM, Culberg R, Schroeder DM, Jordan TM, Seroussi H, Young DA, Blankenship DD and Vaughan
333 DG (2021) Multisystem Synthesis of Radar Sounding Observations of the Amundsen Sea Sector From the
334 2004–2005 Field Season. *Journal of Geophysical Research: Earth Surface*, **126**(10), ISSN 2169-9003, 2169-9011
335 (doi: 10.1029/2021JF006296)
- 336 Creyts TT and Schoof CG (2009) Drainage through subglacial water sheets. *Journal of Geophysical Research*,
337 **114**(F4), F04008, ISSN 0148-0227 (doi: 10.1029/2008JF001215)
- 338 Das I, Morlighem M, Barnes J, Gudmundsson GH, Goldberg D and Dias Dos Santos T (2023) In the Quest
339 of a Parametric Relation Between Ice Sheet Model Inferred Weertman’s Sliding-Law Parameter and Airborne
340 Radar-Derived Basal Reflectivity Underneath Thwaites Glacier, Antarctica. *Geophysical Research Letters*, **50**(10),
341 e2022GL098910, ISSN 0094-8276, 1944-8007 (doi: 10.1029/2022GL098910)
- 342 Dimitrova DS, Kaishev VK and Tan S (2020) Computing the Kolmogorov-Smirnov Distribution When the Underlying
343 CDF is Purely Discrete, Mixed, or Continuous. *Journal of Statistical Software*, **95**(10), ISSN 1548-7660 (doi:
344 10.18637/jss.v095.i10)

Haris and others:

17

- 345 Dowdeswell JA and Evans S (2004) Investigations of the form and flow of ice sheets and glaciers using radio-echo
346 sounding. *Reports on Progress in Physics*, **67**(10), 1821–1861, ISSN 0034-4885, 1361-6633 (doi: 10.1088/0034-
347 4885/67/10/R03)
- 348 Gudmundsson GH (2003) Transmission of basal variability to a glacier surface. *Journal of Geophysical Research:*
349 *Solid Earth*, **108**(B5), 2002JB002107, ISSN 0148-0227 (doi: 10.1029/2002JB002107)
- 350 Habermann M, Maxwell D and Truffer M (2012) Reconstruction of basal properties in ice sheets using iterative inverse
351 methods. *Journal of Glaciology*, **58**(210), 795–808, ISSN 0022-1430, 1727-5652 (doi: 10.3189/2012JoG11J168)
- 352 Hindmarsh RCA (2009) Consistent generation of ice-streams via thermo-viscous instabilities modulated by membrane
353 stresses. *Geophysical Research Letters*, **36**(6), L06502, ISSN 0094-8276 (doi: 10.1029/2008GL036877)
- 354 Hoffman MJ, Perego M, Price SF, Lipscomb WH, Zhang T, Jacobsen D, Tezaur I, Salinger AG, Tuminaro R and
355 Bertagna L (2018) MPAS-Albany Land Ice (MALI): a variable-resolution ice sheet model for Earth system modeling
356 using Voronoi grids. *Geoscientific Model Development*, **11**(9), 3747–3780, ISSN 1991-9603 (doi: 10.5194/gmd-11-
357 3747-2018)
- 358 Holt JW, Blankenship DD, Morse DL, Young DA, Peters ME, Kempf SD, Richter TG, Vaughan DG and
359 Corr HFJ (2006) New boundary conditions for the West Antarctic Ice Sheet: Subglacial topography of the
360 Thwaites and Smith glacier catchments. *Geophysical Research Letters*, **33**(9), L09502, ISSN 0094-8276 (doi:
361 10.1029/2005GL025561)
- 362 Howat I, Porter C, Noh MJ, Husby E, Khuvis S, Danish E, Tomko K, Gardiner J, Negrete A, Yadav B, Klassen J,
363 Kelleher C, Cloutier M, Bakker J, Enos J, Arnold G, Bauer G and Morin P (2022) The Reference Elevation Model
364 of Antarctica - Mosaics, Version 2 (doi: 10.7910/DVN/EBW8UC)
- 365 Hubbard BP, Sharp MJ, Willis IC, Nielsen MK and Smart CC (1995) Borehole water-level variations and the structure
366 of the subglacial hydrological system of Haut Glacier d’Arolla, Valais, Switzerland. *Journal of Glaciology*, **41**(139),
367 572–583, ISSN 0022-1430, 1727-5652 (doi: 10.3189/S0022143000034894)
- 368 Huybrechts P (1990) A 3-D model for the Antarctic ice sheet: a sensitivity study on the glacial-interglacial contrast.
369 *Climate Dynamics*, **5**(2), 79–92, ISSN 0930-7575, 1432-0894 (doi: 10.1007/BF00207423)
- 370 Huybrechts P (2002) Sea-level changes at the LGM from ice-dynamic reconstructions of the Greenland and Antarc-
371 tic ice sheets during the glacial cycles. *Quaternary Science Reviews*, **21**(1-3), 203–231, ISSN 02773791 (doi:
372 10.1016/S0277-3791(01)00082-8)
- 373 Johnson DH (1999) The Insignificance of Statistical Significance Testing. *The Journal of Wildlife Management*, **63**(3),
374 763, ISSN 0022541X (doi: 10.2307/3802789)

Haris and others:

- 375 King EC (2004) Seismic evidence for a water-filled canal in deforming till beneath Rutford Ice Stream, West Antarc-
376 tica. *Geophysical Research Letters*, **31**(20), L20401, ISSN 0094-8276 (doi: 10.1029/2004GL020379)
- 377 Kyrke-Smith TM, Gudmundsson GH and Farrell PE (2017) Can Seismic Observations of Bed Conditions on Ice
378 Streams Help Constrain Parameters in Ice Flow Models?: COMPARISON OF INVERSIONS AND SEISMICS.
379 *Journal of Geophysical Research: Earth Surface*, **122**(11), 2269–2282, ISSN 21699003 (doi: 10.1002/2017JF004373)
- 380 Larson LG (2018) *Investigating Statistical vs. Practical Significance of the Kolmogorov-Smirnov Two-Sample Test*
381 *Using Power Simulations and Resampling Procedures*. Ph.D. thesis
- 382 Lipscomb WH, Price SF, Hoffman MJ, Leguy GR, Bennett AR, Bradley SL, Evans KJ, Fyke JG, Kennedy JH,
383 Perego M, Ranken DM, Sacks WJ, Salinger AG, Vargo LJ and Worley PH (2019) Description and evaluation of
384 the Community Ice Sheet Model (CISM) v2.1. *Geoscientific Model Development*, **12**(1), 387–424, ISSN 1991-9603
385 (doi: 10.5194/gmd-12-387-2019)
- 386 MacAyeal DR (1992) The basal stress distribution of Ice Stream E, Antarctica, inferred by control methods. *Journal*
387 *of Geophysical Research*, **97**(B1), 595, ISSN 0148-0227 (doi: 10.1029/91JB02454)
- 388 MacAyeal DR (1993) A tutorial on the use of control methods in ice-sheet modeling. *Journal of Glaciology*, **39**(131),
389 91–98, ISSN 0022-1430, 1727-5652 (doi: 10.3189/S0022143000015744)
- 390 Mantelli E and Schoof C (2019) Ice sheet flow with thermally activated sliding. Part 2: the stability of subtem-
391 perate regions. *Proceedings of the Royal Society A: Mathematical, Physical and Engineering Sciences*, **475**(2231),
392 20190411, ISSN 1364-5021, 1471-2946 (doi: 10.1098/rspa.2019.0411)
- 393 Mantelli E, Haseloff M and Schoof C (2019) Ice sheet flow with thermally activated sliding. Part 1: the role of advec-
394 tion. *Proceedings of the Royal Society A: Mathematical, Physical and Engineering Sciences*, **475**(2230), 20190410,
395 ISSN 1364-5021, 1471-2946 (doi: 10.1098/rspa.2019.0410)
- 396 Morlighem M (2022) MEaSURES BedMachine Antarctica, Version 3 (doi: 10.5067/FPSU0V1MWUB6)
- 397 Morlighem M, Rignot E, Seroussi H, Larour E, Ben Dhia H and Aubry D (2010) Spatial patterns of basal drag
398 inferred using control methods from a full-Stokes and simpler models for Pine Island Glacier, West Antarctica:
399 SPATIAL PATTERNS OF BASAL DRAG. *Geophysical Research Letters*, **37**(14), n/a–n/a, ISSN 00948276 (doi:
400 10.1029/2010GL043853)
- 401 Morlighem M, Rignot E, Binder T, Blankenship D, Drews R, Eagles G, Eisen O, Ferraccioli F, Forsberg R, Fretwell
402 P, Goel V, Greenbaum JS, Gudmundsson H, Guo J, Helm V, Hofstede C, Howat I, Humbert A, Jokat W, Karlsson
403 NB, Lee WS, Matsuoka K, Millan R, Mouginot J, Paden J, Pattyn F, Roberts J, Rosier S, Ruppel A, Seroussi H,
404 Smith EC, Steinhage D, Sun B, Broeke MRVD, Ommen TDV, Wessem MV and Young DA (2020) Deep glacial

- 405 troughs and stabilizing ridges unveiled beneath the margins of the Antarctic ice sheet. *Nature Geoscience*, **13**(2),
406 132–137, ISSN 1752-0894, 1752-0908 (doi: 10.1038/s41561-019-0510-8)
- 407 Mouginit J, Rignot E, Scheuchl B and Millan R (2017) Comprehensive Annual Ice Sheet Velocity Mapping
408 Using Landsat-8, Sentinel-1, and RADARSAT-2 Data. *Remote Sensing*, **9**(4), 364, ISSN 2072-4292 (doi:
409 10.3390/rs9040364)
- 410 Pattyn F, Favier L, Sun S and Durand G (2017) Progress in Numerical Modeling of Antarctic Ice-Sheet Dynamics.
411 *Current Climate Change Reports*, **3**(3), 174–184, ISSN 2198-6061 (doi: 10.1007/s40641-017-0069-7)
- 412 Payne AJ, Huybrechts P, Abe-Ouchi A, Calov R, Fastook JL, Greve R, Marshall SJ, Marsiat I, Ritz C, Tarasov L
413 and Thomassen MPA (2000) Results from the EISMINT model intercomparison: the effects of thermomechanical
414 coupling. *Journal of Glaciology*, **46**(153), 227–238, ISSN 0022-1430, 1727-5652 (doi: 10.3189/172756500781832891)
- 415 Peters M, Blankenship D, Carter S, Kempf S, Young D and Holt J (2007) Along-Track Focusing of Airborne Radar
416 Sounding Data From West Antarctica for Improving Basal Reflection Analysis and Layer Detection. *IEEE Trans-*
417 *actions on Geoscience and Remote Sensing*, **45**(9), 2725–2736, ISSN 0196-2892 (doi: 10.1109/TGRS.2007.897416)
- 418 Peters ME (2005) Analysis techniques for coherent airborne radar sounding: Application to West Antarctic ice
419 streams. *Journal of Geophysical Research*, **110**(B6), B06303, ISSN 0148-0227 (doi: 10.1029/2004JB003222)
- 420 Pfeffer WT, Humphrey NF, Amadei B, Harper J and Wegmann J (2000) In situ stress tensor measured in an Alaskan
421 glacier. *Annals of Glaciology*, **31**, 229–235, ISSN 0260-3055, 1727-5644 (doi: 10.3189/172756400781820354)
- 422 Pollard D and DeConto RM (2012) A simple inverse method for the distribution of basal sliding coefficients under
423 ice sheets, applied to Antarctica. *The Cryosphere*, **6**(5), 953–971, ISSN 1994-0424 (doi: 10.5194/tc-6-953-2012)
- 424 Pritchard HD, Arthern RJ, Vaughan DG and Edwards LA (2009) Extensive dynamic thinning on the margins of the
425 Greenland and Antarctic ice sheets. *Nature*, **461**(7266), 971–975, ISSN 0028-0836, 1476-4687 (doi: 10.1038/na-
426 ture08471)
- 427 Ranganathan M, Minchew B, Meyer CR and Gudmundsson GH (2021) A new approach to inferring basal drag
428 and ice rheology in ice streams, with applications to West Antarctic Ice Streams. *Journal of Glaciology*, **67**(262),
429 229–242, ISSN 0022-1430, 1727-5652 (doi: 10.1017/jog.2020.95)
- 430 Raymond MJ and Gudmundsson GH (2005) On the relationship between surface and basal properties on
431 glaciers, ice sheets, and ice streams. *Journal of Geophysical Research*, **110**(B8), B08411, ISSN 0148-0227 (doi:
432 10.1029/2005JB003681)
- 433 Rignot E and University Of California Irvine (2017) MEaSURES Annual Antarctic Ice Velocity Maps, 2006-2017,
434 Version 1 (doi: 10.5067/9T4EPQXTJYW9)

- 435 Schoof C (2006) Variational methods for glacier flow over plastic till. *Journal of Fluid Mechanics*, **555**, 299, ISSN
436 0022-1120, 1469-7645 (doi: 10.1017/S0022112006009104)
- 437 Schoof C (2007) Ice sheet grounding line dynamics: Steady states, stability, and hysteresis. *Journal of Geophysical*
438 *Research*, **112**(F3), F03S28, ISSN 0148-0227 (doi: 10.1029/2006JF000664)
- 439 Schoof C (2010) Ice-sheet acceleration driven by melt supply variability. *Nature*, **468**(7325), 803–806, ISSN 0028-0836,
440 1476-4687 (doi: 10.1038/nature09618)
- 441 Schroeder DM, Blankenship DD and Young DA (2013) Evidence for a water system transition beneath Thwaites
442 Glacier, West Antarctica. *Proceedings of the National Academy of Sciences*, **110**(30), 12225–12228, ISSN 0027-
443 8424, 1091-6490 (doi: 10.1073/pnas.1302828110)
- 444 Schroeder DM, Blankenship DD, Raney RK and Grima C (2015) Estimating Subglacial Water Geometry Using
445 Radar Bed Echo Specularity: Application to Thwaites Glacier, West Antarctica. *IEEE Geoscience and Remote*
446 *Sensing Letters*, **12**(3), 443–447, ISSN 1545-598X, 1558-0571 (doi: 10.1109/LGRS.2014.2337878)
- 447 Sergienko OV and Hindmarsh RCA (2013) Regular Patterns in Frictional Resistance of Ice-Stream Beds Seen by
448 Surface Data Inversion. *Science*, **342**(6162), 1086–1089, ISSN 0036-8075, 1095-9203 (doi: 10.1126/science.1243903)
- 449 Sergienko OV, Bindschadler RA, Vornberger PL and MacAyeal DR (2008) Ice stream basal conditions from block-wise
450 surface data inversion and simple regression models of ice stream flow: Application to Bindschadler Ice Stream.
451 *Journal of Geophysical Research*, **113**(F4), F04010, ISSN 0148-0227 (doi: 10.1029/2008JF001004)
- 452 Seroussi H, Morlighem M, Rignot E, Khazendar A, Larour E and Mouginot J (2013) Dependence of century-scale
453 projections of the Greenland ice sheet on its thermal regime. *Journal of Glaciology*, **59**(218), 1024–1034, ISSN
454 0022-1430, 1727-5652 (doi: 10.3189/2013JoG13J054)
- 455 Seroussi H, Nowicki S, Payne AJ, Goelzer H, Lipscomb WH, Abe-Ouchi A, Agosta C, Albrecht T, Asay-Davis X,
456 Barthel A, Calov R, Cullather R, Dumas C, Galton-Fenzi BK, Gladstone R, Golledge NR, Gregory JM, Greve R,
457 Hattermann T, Hoffman MJ, Humbert A, Huybrechts P, Jourdain NC, Kleiner T, Larour E, Leguy GR, Lowry
458 DP, Little CM, Morlighem M, Pattyn F, Pelle T, Price SF, Quiquet A, Reese R, Schlegel NJ, Shepherd A, Simon
459 E, Smith RS, Straneo F, Sun S, Trusel LD, Van Breedam J, van de Wal RSW, Winkelmann R, Zhao C, Zhang T
460 and Zwinger T (2020) ISMIP6 Antarctica: a multi-model ensemble of the Antarctic ice sheet evolution over the
461 21st century. *The Cryosphere*, **14**(9), 3033–3070, ISSN 1994-0424 (doi: 10.5194/tc-14-3033-2020)
- 462 Smith AM (1997) Basal conditions on Rutford Ice Stream, West Antarctica, from seismic observations. *Journal of*
463 *Geophysical Research: Solid Earth*, **102**(B1), 543–552, ISSN 01480227 (doi: 10.1029/96JB02933)

- 464 Sullivan GM and Feinn R (2012) Using Effect Size—or Why the P Value Is Not Enough. *Journal of Graduate Medical*
465 *Education*, **4**(3), 279–282, ISSN 1949-8357, 1949-8349 (doi: 10.4300/JGME-D-12-00156.1)
- 466 Tulaczyk SM and Foley NT (2020) The role of electrical conductivity in radar wave reflection from glacier beds. *The*
467 *Cryosphere*, **14**(12), 4495–4506, ISSN 1994-0424 (doi: 10.5194/tc-14-4495-2020)
- 468 Vaughan DG, Corr HFJ, Ferraccioli F, Frearson N, O’Hare A, Mach D, Holt JW, Blankenship DD, Morse DL and
469 Young DA (2006) New boundary conditions for the West Antarctic ice sheet: Subglacial topography beneath Pine
470 Island Glacier. *Geophysical Research Letters*, **33**(9), L09501, ISSN 0094-8276 (doi: 10.1029/2005GL025588)
- 471 Walder JS and Fowler A (1994) Channelized subglacial drainage over a deformable bed. *Journal of Glaciology*,
472 **40**(134), 3–15, ISSN 0022-1430, 1727-5652 (doi: 10.3189/S0022143000003750)
- 473 Winkelmann R, Martin MA, Haseloff M, Albrecht T, Bueler E, Khroulev C and Levermann A (2011) The Potsdam
474 Parallel Ice Sheet Model (PISM-PIK) – Part 1: Model description. *The Cryosphere*, **5**(3), 715–726, ISSN 1994-0424
475 (doi: 10.5194/tc-5-715-2011)
- 476 Wolovick M, Humbert A, Kleiner T and Rückamp M (2023) Regularization and L-curves in ice sheet inverse models: a
477 case study in the Filchner–Ronne catchment. *The Cryosphere*, **17**(12), 5027–5060, ISSN 1994-0424 (doi: 10.5194/tc-
478 17-5027-2023)
- 479 Young DA, Schroeder DM, Blankenship DD, Kempf SD and Quartini E (2016) The distribution of basal water between
480 Antarctic subglacial lakes from radar sounding. *Philosophical Transactions of the Royal Society A: Mathematical,*
481 *Physical and Engineering Sciences*, **374**(2059), 20140297 (doi: 10.1098/rsta.2014.0297)
- 482 Zhao C, Gladstone RM, Warner RC, King MA, Zwinger T and Morlighem M (2018) Basal friction of Fleming
483 Glacier, Antarctica – Part 1: Sensitivity of inversion to temperature and bedrock uncertainty. *The Cryosphere*,
484 **12**(8), 2637–2652, ISSN 1994-0424 (doi: 10.5194/tc-12-2637-2018)